Proceedings of the ASME 2010 3rd Joint US-European Fluids Engineering Summer Meeting and 8th International Conference on Nanochannels, Microchannels, and Minichannels
FEDSM-ICNMM2010
August 1-5, 2010, Montreal, Canada

FEDSM-ICNMM2010-30794

EXPERIMENTAL CHARACTERIZATION OF AEROSOL FLOW THROUGH A MICRO-CAPILLARY

Zakaria MAHMUD, Justin M. HOEY, Artur LUTFURAKHMANOV, Jason DAUGS, Orven F. SWENSON, Douglas L. SCHULZ, Iskander S. AKHATOV

North Dakota State University, Fargo, ND, 58108, USA

ABSTRACT

Aerosol flow through a long and tapered micro-capillary (MC) for direct write (DW) technology is typically used with small particles of sizes ranging from 0.2 µm to 10 µm at velocities up to 100 m/s. Earlier research showed that the particles coming through a long MC experience Saffman force that moves the particles towards the center of the beam other than the geometric convergence (due to Stokes drag); thus creating a collimated aerosol beam. It was also established that the additional Saffman force becomes more effective with certain particle diameters and velocities. Therefore, for experimental validation, it is important to accurately measure the particle size distribution and velocities coming out of the long MC. However, the current sizing methods are incapable of measuring particles less than 5 µm due to optical limitations. The current paper presents results using a micro-shadowgraphy system from LaVision Inc. to characterize the flow field. A modification of the particle-sizing algorithm is proposed to measure particles of sub-micron sizes. The modified algorithm can be used to accurately size particles of 1µm diameter.

Keywords: Aerosol, Micro-Shadowgraphy, Focusing, Direct-Write

1. INTRODUCTION

Measurement of the particle sizes and the speed of an aerosol flow are crucial for a number of applications. One important application is medical inhalers where particle size distributions of the doses determine the deposition location in the respiratory tract. Deposition in the oropharyngeal region requires particle sizes > 6µm, in the bronchial region requires sizes between 1 to 6 µm, and in alveolar region requires particle sizes between 0.4 to 1 µm [1]. Another application of aerosol flow is the direct write (DW) technologies, where particle size distribution is an important parameter that governs the quality of the printed lines. Depending on the ink-properties, the particle sizes of the DW aerosol jet varies from 0.2 µm to 5 µm creating line-widths of 5 µm to 5 mm [2]. In addition to the particle sizes, the velocity components of the aerosol beam are also paramount in creating thin, uniform, and continuous lines. The jet velocity determines how well the beam is focused and collimated. Therefore, characterization of the aerosol flow for the particle sizes, velocities, and often concentration are required for specific applications.

The measurement methods to determine particle size & velocity can be grouped into three broad categories: a) Mechanical, b) Electrical, and c) Optical. Mechanical methods generally include drop collection on slides, molten wax, and frozen drop techniques; the electrical methods include charged wire and hot-wire techniques; and the optical methods include imaging techniques (Particle/ Droplet Image Analysis PDIA, sizing master shadowgraphy) and non-imaging techniques (Phase Doppler Anemometry (PDA), Shadow Doppler Velocimetry (SDV)). Lefebvre [3] in 1989 gave a detailed description of each category with its relative advantages and disadvantages. Optical methods were popular mainly due to the advancement in imaging technology and computing capability. Until recently, PDA was considered the most accurate particle sizing method and was widely used for low-speed aerosol characterization. PDA uses scattered light from the droplets to measure size and velocities. The system accuracy depends mostly on the precise optical alignment, particle diameter, and most importantly the sphericity of the particles. The method works better with larger particle sizes, because the scattered light is proportional to the square of the droplet diameter. In addition, the system is incapable of measuring non-spherical particles, therefore the measurement location is normally chosen far downstream of the aerosol nozzle to ensure better sphericity. The SDV technique on the other hand can measure non-spherical particles with reasonable accuracy and works well with larger particles, but the system has limited size dynamic range. The direct imaging techniques (PDIA, or micro-shadowgraphy) can overcome the limitations associated with the light scattering techniques. Kashdan et al. [4] demonstrated that PDIA system is capable of measuring particle sizes in the range of 10 to 30 μm with speeds of up to 50 m/s. Finally, the micro-shadowgraphy technique from Lavision Inc. is specified for measuring particle sizes of 5 μm or larger at wide velocity ranges. In addition, the micro-shadowgraphy system can be integrated with a long working distance (32 to 341mm) microscopic lens, which makes the system unique for high-speed spray characteristics.

The present paper investigates the aerosol flow through a 1cm long tapered nozzle with the inlet and exit diameters of 800 μm and 125 μm respectively referred to as the Micro Capillary (MC). Akhatov et al. [5,7] investigated the aerosol flow through MC and concluded that the Stokes and Saffman forces are the major contributors to the collimation of an aerosol beam with an exit velocity of about 100 m/s. The details of the aerosol deposition method with particular interest in focusing of the beam for Direct Write are discussed in [6].

Measuring sizes and velocities of particles in high-speed flight poses significant experimental challenges. Aerosol flow through a MC is an example of a flow field, where depending on the conditions the particle sizes may vary from 0.2 micron to 1 mm with speeds up to 100 m/s.

In Section 2 the current limitations in the image based particle sizing techniques are discussed. These limitations are mainly due to the diffraction-limited resolution, 2D data recorded from a 3D measurement volume, varying depth of field depending on particle size, and the high-speed flow of the particles. In Section 3, a detailed description of the micro-shadowgraphy system is given with operating conditions to measure the particle statistics. The particle statistics and results are discussed in Section 4. The suggested modification and the importance of the further research requirement on the current algorithm are discussed in Section 5. The conclusion is given in Section 6.

2. UNDERSTANDING THE LIMITATIONS IN OPTICAL MEASUREMENT METHODS

Particle sizing techniques used today often rely on optical methods with direct imaging which works well if the particles measured are large in size (> 10 μm), located near the object plane of the imaging system, and fly at low-velocity. The aerosol flows in numerous applications typically have particles of 0.2 μm to about 1 mm in diameter, and often flow at high-speed of ~100 m/s. Therefore, it is important to understand the limitation in measuring small particles (less than 5 μm) in a high-speed aerosol flow. Some of these limitations are discussed below.

Diffraction limited resolution: For microscopic imaging, diffraction limited resolution is also referred to as the resolving power of a lens. Meinhart & Wereley [8] explained that a point light source if imaged by a single air-immersion lens will give the diffraction limited spot size,

$$d_s = 1.22(M+1)\frac{\lambda}{NA}$$

Here M is magnification, λ is wavelength, and NA is the numerical aperture of the objective lens. However, as presented by Breuer [9], the effective image diameter,

$$d_e = \sqrt{d_s^2 + M^2 d_p^2}$$

Here d_p is particle diameter. It is also explained in [9], that using a conventional microscope with NA=1.4, particle diameters ≤ 0.2 μm will provide image resolution of $d_e / M \sim 0.3$ μm, while for an air-immersion lens with $M = 10$, and $NA = 0.25$, particle diameters ≤ 1.0 μm will be diffraction limited. For the current micro-shadowgraphy experimental facility the diffraction limited spot size can be estimated as 2.6 μm with wavelength 600 nm, NA= 0.28 and magnification 37.4.

Out-of-plane spatial resolution: In micro-PIV, 3D measurement volume is used to capture a 2D image for statistical measurements. For shadow-imaging techniques, 3D diffraction pattern is observed for the particles in the measurement volume. The thickness of the object plane from the 3D volume can be defined as the depth of field of the system. Following Meinhart et al [10] and Stone et al [11], the depth of field is

$$\delta z = \frac{n^2\lambda}{NA^2} + \frac{ne}{NA}M^{-1}$$

Here, n is refractive index of the medium, e is the smallest distance that can be resolved by the image plane (space between pixels). Thus, the depth of field depends on the diffraction and the geometric effects. For measuring particle sizes from the shadow imaging, the algorithm is equipped with the depth of field correction. Kim & Kim [12] experimentally calibrated the depth of field for specific particle sizes by using normalized contrast of the local and background gray levels and the slopes of the shadow-edges. They also introduced an algorithm to estimate the particle sizes from the shadow images based on their normalized gray levels and edge-sharpness. The algorithm was proved very accurate for particle sizes of 3.9 to 71.7 μm diameters.

High-speed: high-speed imaging of a micron scale field of view requires very small delay time settings to capture particles for two-frame velocity measurements. However, with a small field of view, the light-intensity is reduced, which requires an image-intensifier to capture particles. In addition, for high-speed gases the particles do not follow the gas unless the particle-sizes are sufficiently small (about < 0.2 μm). However as mentioned earlier, particles this small cannot be imaged easily for velocity estimation due to diffraction limited optics.

3. MICRO-SHADOWGRAPHY SYSTEM

Experimental characterization of the aerosol flow out of the MC was accomplished with a micro-shadowgraphy system, purchased from LaVision Inc. that uses pulsed backlight illumination and high magnification imaging to capture shadows of the particles that are in the measurement volume of the imaging system. The system is designed to provide particle sizes of diameter greater than 5 μm and 2D planar velocity components. The expected size of the particles in this experiment ranged from 1 to 10 μm in diameter with the majority particles below 5 μm. Therefore, the ability of the system to size these particles was in question. A detailed description of the experimental set-up and procedure is given below.

3.1. Experimental Facility and Setup

The micro-shadowgraphy system from LaVision Inc. consists of a pulsed backlight illumination system coupled with high-magnification imaging optics. The backlight illumination system is comprised of: 1) Quantel USA Inc. dual cavity Nd:YAG 532 nm Q-switched laser - 120 mJ/pulse, 10 ns pulse duration; 2) high efficiency dye plate diffuser which converts the 532 nm laser beam to 600 nm incoherent light at 30% conversion efficiency; 3) liquid fiber optic delivery system; and 4) 120 mm Fresnel lens. To facilitate data collection, a 532 nm CW laser was used with the micro-shadowgraphy system. The imaging system components are: 1) Imager Intense CCD camera - 1376 × 1040 pixel resolution, maximum frame rate of 10 Hz, 12-bit output, 6.45 × 6.45 μm pixels, and minimum adjustable time between frames of 0.5 μs; and 2) Magnification Optics: a 12X Navitar UltraZoom lens, 2X doubling optics, and an Olympus 10X long working distance objective. The total magnification of the system ranged from 5.8X to 140X with a minimum field of view of ~100 μm.

Figure 1 shows a drawing of the set-up. The Fresnel lens and the camera were mounted on a rail with carriers that provided course adjustment as needed to position the camera and the background light source (Fresnel lens). For convenience, the aerosol beam was positioned in the center of the camera field of view and was focused with a three-dimensional translation stage and micrometers. A CW laser (shown in Figure 1) and a manually controlled translation stage were used to position the aerosol beam within the field of view (*x* – and *y* – positions) of the imaging system. Two Thorlabs LT series stages with 50 mm travel and a coarse and fine adjustment of 1.397 and 0.254 mm per revolution, respectively were used to adjust *x*- and *y*-positions, while a precision motorized actuator (Thorlabs LTA-HS stage with 50 mm travel, 0.035 μm resolution, and 0.15 μm repeatability) was used to position the aerosol beam in the depth of field (*z* – position).

Aerosol was generated through the atomization of a mixture consisting of 0.25 mL Ag nanoparticles and 0.5 mL deionized water via a piezoelectric atomizer. This mixture was contained in a glass collection vial partially submerged in an ultrasonic water bath. The bath temperature was monitored with a handheld infrared thermometer. The temperature was maintained between 28 °C and 32 °C by the addition of ice to the ultrasonic bath.

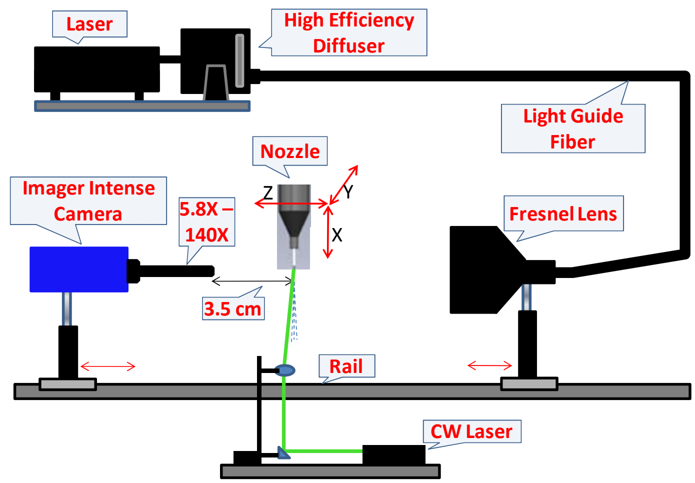

Figure 1. Diagram of Micro-Shadowgraphy system for visualizing aerosol particles.

The seeded aerosol particles with nitrogen as carrier gas were then routed through a deposition head purchased from Optomec Inc., mixed annularly with a sheath gas (nitrogen), and focused through a linearly converging alumina nozzle (manufactured by CoorsTek Inc.) with the dimensions shown in Figure 2.

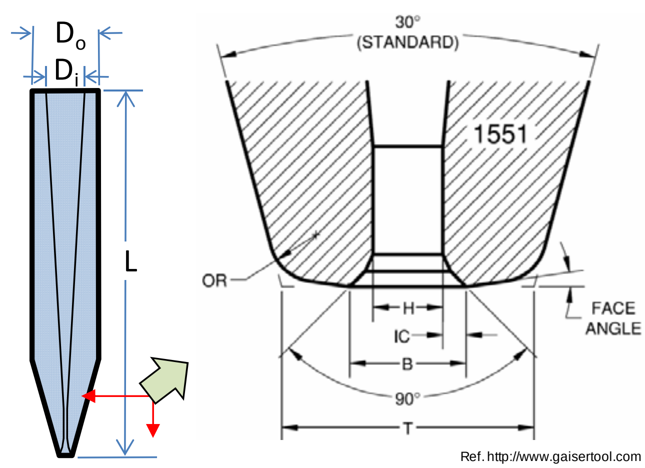

Figure 2. Nozzle Dimensions: L = 1.9 cm; D_0 = 1.6 mm; D_i = 800 μm; H = 127 μm; IC = 3.81 μm; T = 508 μm; Face Angle = Flat

The total volumetric flow rate through the nozzle was 40 ± 2.5 sccm, maintained by a pair of MKS Type M100B mass flow controllers, each with an uncertainty of 1 % FS. Carrier and sheath volumetric flow rates were 20 ± 1.25 sccm each. The pressure measured in the carrier gas line exiting the mass flow controller was 2.9 kPa to 3.1 kPa throughout the duration of the experiment.

The micro-shadowgraphy system was equipped with Davis 7.2 software to record and analyze data. The following parameters were used to record experimental data of the aerosol beam. The optical magnification ~ 80X provided an image length scale of 5.8 pixels per µm. The field of view had dimensions of 238 × 180 µm. The tip of the nozzle was positioned directly above the field of view. Two sets of 10,000 double-frame experimental images were recorded at 5 Hz. Thus, the total runtime of each set of the experiment was about 33 minutes. The time between individual frames was set to 0.6 µs, which provided a particle displacement of about 50 µm. The system was sensitive to the background illumination intensity and uniformity, therefore the laser power was chosen to achieve uniform steady background illumination of about 2000 counts in both frames. It was also observed that the background illumination decayed over time due to degradation of the diffuser dye, therefore to maintain illumination intensity, the second set of experimental images required an increased laser power. For each set of experimental images, 100 reference images were recorded for image preprocessing, discussed below.

3.2 Algorithm for Particle Sizing and Velocity Measurement

For particle size and velocity calculation, the algorithm operated in three steps: 1) the software detected the existence of possible particles in the image (this step is called first segmentation), 2) the software estimated the particle diameter and location (this step is called second segmentation), and 3) the software calculated velocity from the particle displacement between frames. These steps are discussed in details below.

Detection of particles in the image (first segmentation): An average reference image was created from images recorded with no particles present. To minimize background noise due to non-uniform illumination, the raw images with particles present were then subtracted from and normalized by this averaged reference image to create normalized inverted images. The absolute maximum intensity would correspond to a particle with a complete shadow (camera signal of zero). The intensities displayed in Figure 3 (left axis) correspond to those normalized to the absolute maximum intensity. The parameter global threshold, which was set to 35% of the absolute maximum intensity, was used to identify all the pixels that have higher intensities than the global threshold. In Figure 3, the particle's greatest intensity is 80% of the absolute maximum intensity (left axis). The green dashed line represents the global threshold.

Particle sizing and position (second segmentation): Adjacent pixels above the global threshold were bounded by a rectangle containing those pixels (Area of Interest, AOI). The AOI was then expanded by 200 %. The intensities of the pixels within this expanded AOI were then normalized by the maximum intensity of those pixels. The pixels were then divided into two areas which were defined by whether the intensities exceeded the low or high level thresholds, see right axis on Figure 3.

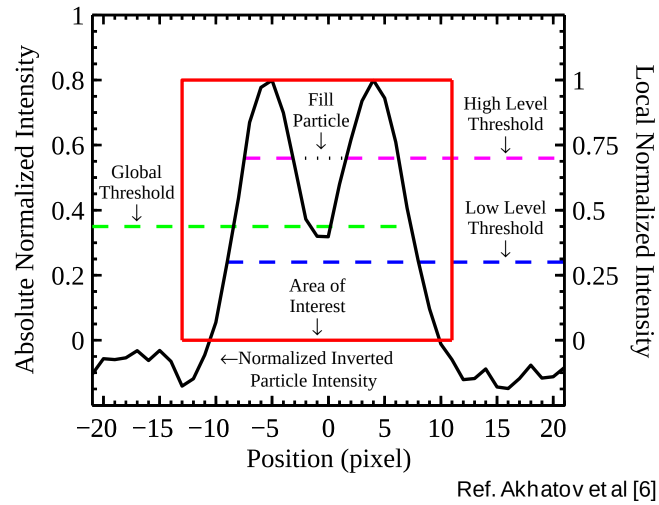

Figure 3. Intensity profile of a particle demonstrating the first (left axis) and second (right axis) particle segmentation.

The high and low level diameters were calculated from the corresponding areas, assuming a circular particle. The particle diameter was calculated as the average of the high and low level diameters. Due to diffraction around the particle, the intensities at the center of some particle areas are lower than their bordering pixels (see Figure 3). To correct for this, the algorithm "fills" this dip by counting these pixels in the high-level area rather than in the low-level area. The particle position was calculated as the center of the expanded AOI. The ratio of the low to high level area indicated how close a particle was to the object plane of the imaging system. The particle was ignored for measurement purposes if: 1) the number of pixels in the low level area was greater than three times the number in the high level area, 2) the centricity of the particle was less than 60 %, or 3) the particle was touching the border of the field of view.

Velocity calculation: The micro-shadowgraphy system provides a velocity distribution for different size classes. Unlike PIV (Particle Image Velocimetry), or PTV (Particle Tracking Velocimetry), this method validates the velocity vector based on the particle displacement and size deviation between frames. Due to the challenge associated with sizing small particles (as mentioned earlier), a restriction of 15% diameter deviation between frames was used. This resulted in a validated detection of the particle in the two corresponding frames. Due to the scarcity of particles, a larger particle shift between frames was acceptable. This large shift increased the accuracy of velocity measurement. Even though this parameter was set in the software an occasional incorrect velocity vector would be found due to the wrong pair of particles. To correct for these bad velocity vectors, post processing was done on Matlab that set a bound for the velocity with a maximum and minimum value.

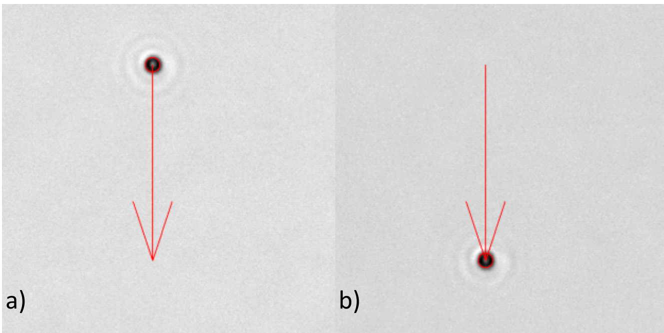

Figure 4. Image of an aerosol particle in the a) first frame, b) second frame of shadowgraphy.

Figure 4 depicts: a) the first frame of the image, and b) the second frame of the image. The displacement of the particle and the time between frames were used to calculate the velocity. The initial interrogation window for the velocity calculation was 100 × 100 µm, and then decreased to 50 × 50 µm in the next pass.

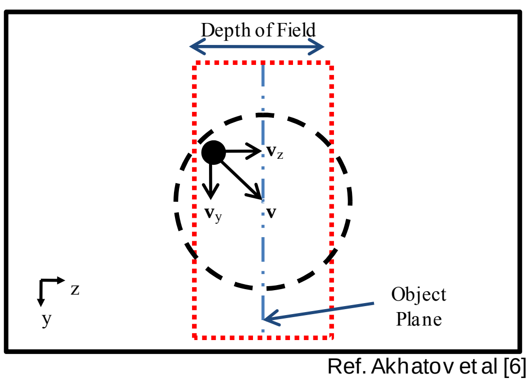

Figure 5. Diagram showing the systematic error in radial velocity measurements due to the depth of field.

The micro-shadowgraphy technique captures only the planar velocity of the particles, therefore creating a systematic error in the measurements of the actual radial velocities due to the depth of field. In Figure 5, the particle is shown in a z-axis position that is out of focus but detectable by the camera. Although the axial component of the measured velocity will be correct, the radial component will be the projection of the actual radial velocity on the object plane. The axial and radial velocities are the projections along the x-axis and onto the y-z plane respectively. Because the image is in 2D in the x-y plane, the z-component of the radial velocity is not detected. This error could be minimized by narrowing the depth of field by optical means or by software restrictions on particle validation, thereby effectively reducing the depth of field.

4. RESULTS: AEROSOL CHARACTERIZATION

The particle size, velocity and number densities were experimentally obtained for the flow through a long MC. The experimental results and challenges associated with the aerosol characterization are discussed below.

4.1 Detection of the Beam Center

The particle distribution across the aerosol beam is expected to be about Gaussian; however it was observed that the particle density was consistently skewed with higher density in the positive *y*-axis. This may have been caused by gravitational sedimentation of the particles in the tube between the atomizer and the deposition head. Once the tube-length between the atomizer and the deposition head was minimized (by relocating the atomizer), the particle density was found stably Gaussian.

To find the center plane of the beam, data were taken by traversing the deposition head in 5 µm increments along the *z* – axis (see Figure 6). The plane at the *z* – position which corresponded to the image containing the maximum beam width and maximum number of detected particles was considered as passing through the center of the aerosol beam.

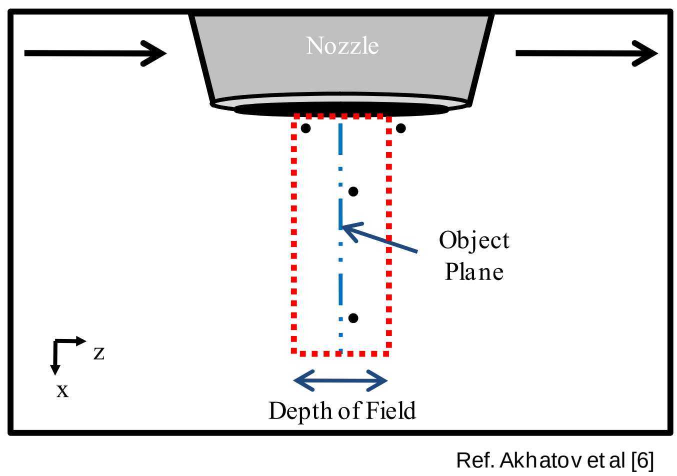

Figure 6. Schematic displaying the method used to align the center of the aerosol beam with the focal plane.

However, the technique was time consuming and tedious. Therefore, a CW laser (shown in schematic, Figure 1) was used to manually find the focused and centered aerosol beam by volume-illuminating the particles for long exposure times (about 80-100 ms). First, the deposition head was moved along the *y*-axis to place the beam in the center of the field of view of the camera and then it was moved in the *z*-axis in 5 µm steps to find the sharpest focused image of the particle streak lines (see Figure 7). This *z*-location corresponds to the location of the beam center.

The focused image obtained with the CW laser was then verified with the shadowgraphy images that were taken in 5 µm increments along the *z* – axis. For each location, the number of particles and the beam width were recorded and plotted, as shown in Figure 8. The radial location with the maximum number of particles and the largest beam width matched and indicated the beam center.

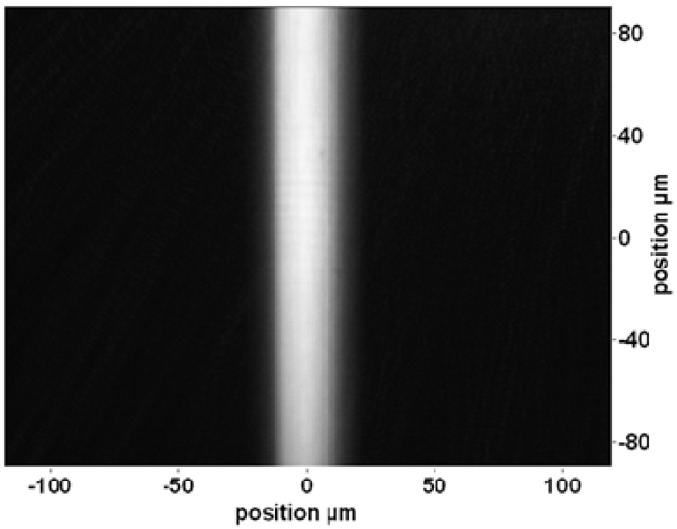

Figure 7. CW laser scattering from aerosol beam. MC outlet diameter 125 micrometers.

The zero position in Figure 8 corresponds to the focused scattering image from the CW laser, while the position at 10 µm indicates the location of the beam center determined by the particle distribution obtained with the shadow images. Further analysis revealed that the CW laser focusing is within 5 to 10 µm of the actual center.

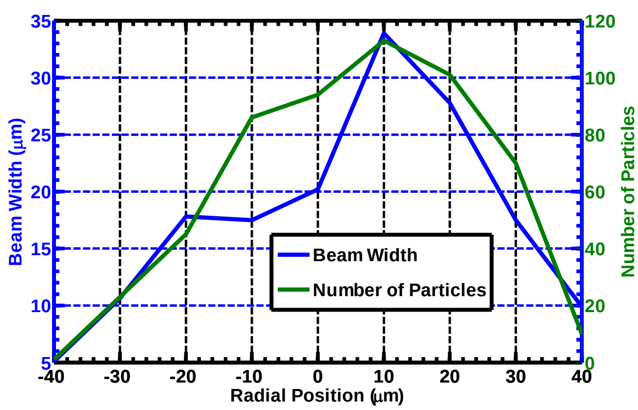

Figure 8. Beam width and number of particles vs radial position.

4.2 Axial velocity profile downstream from the nozzle exit

Figure 9 shows the axial velocity profiles of the aerosol stream away from the nozzle along the x-axis. Eight measurement locations at 318 µm apart (corresponding to one revolution of the coarse adjustment screw) were chosen to create the profile. The zero position in the graph is the nozzle exit. The profile shows that the particles are accelerated until 1 mm downstream and then start to slow down. This phenomenon was later justified by the modeling the gas velocities showing that the gas velocity exceeds the particle velocities beyond the nozzle exit, further accelerating the particles.

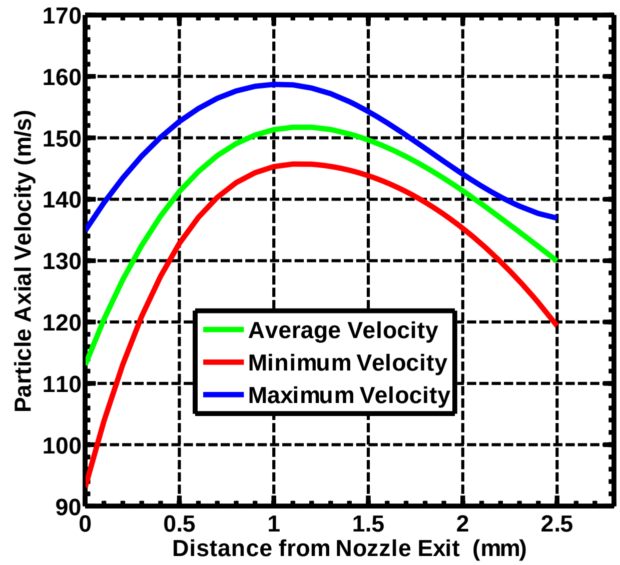

Figure 9. Average axial velocities of aerosol particles versus distance from the nozzle exit.

4.3 Aerosol statistics

Particle density distribution: Figure 10 shows the particle density for a 125 µm nozzle exit diameter right at the nozzle exit. Here the beam center from the CW laser is located at 0 µm. The density plot shows an asymmetric distribution with higher particle densities on the left. The maximum density location (at -10 µm), if assumed to be the actual beam center, is still within 10 µm from the predicted beam center location, which was expected because the centering was done with the CW laser with 5 to 10 µm uncertainty.

The size distribution: Details on particle sizing will be discussed in the next section. With the existing algorithm, the size distribution plot shown in Figure 11 reveals that the particle diameter varied from 1.4 to 8 µm with a mean value of 2.5 µm. The particle detection algorithm is specified for particle sizes 5 µm or larger, however the majority of particles in the size distribution indicate sizes smaller than 5 µm. Depending on the parameters used, the software often predicts incorrect particle sizes, as shown in the Figure 12. Here, 5 µm polystyrene particles mounted on glass slides were imaged at approximately 14 microns from the object plane of the imaging system. Only 6 pixels (see below) were observed above the global threshold (80%). Thus the AOI expansion of 80% captures only a small portion of the particle image area. The red circle is drawn to show the approximate difference between the actual size and the calculated size. Another instance is shown in

Figure 13, where for the same particle, an AOI expansion of 500% was used and still the calculated diameter is about one half of the actual imaged particle.

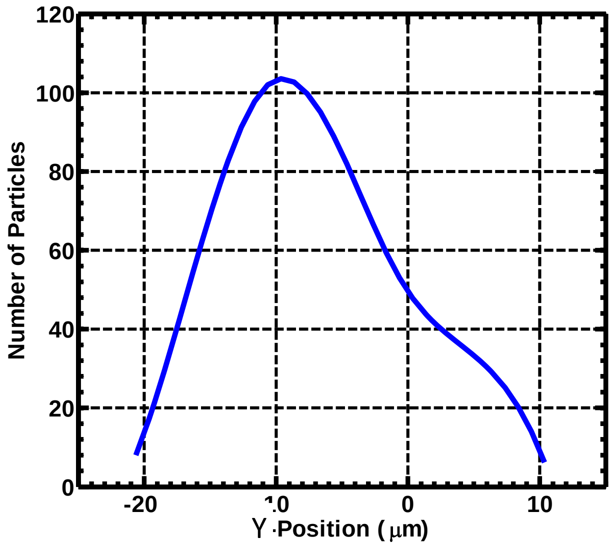

Figure 10. Particle density profile in radial location.

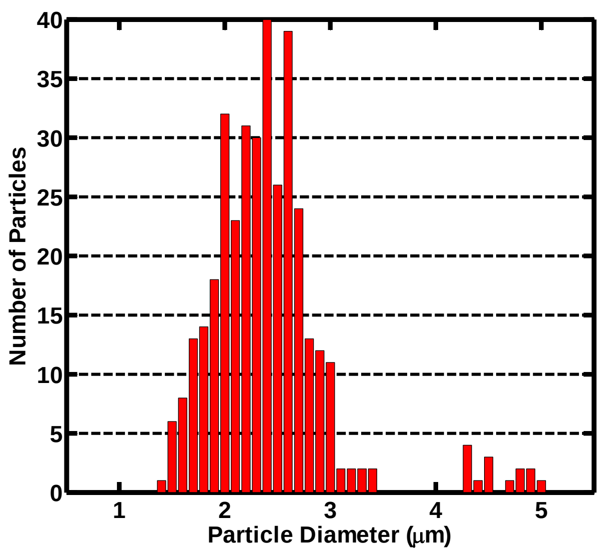

Figure 11. Particle size distribution.

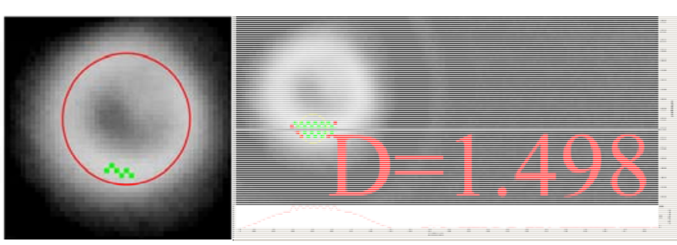

Global Segmentation Particle segmentation

Figure 12. Global and particle segmentation images.

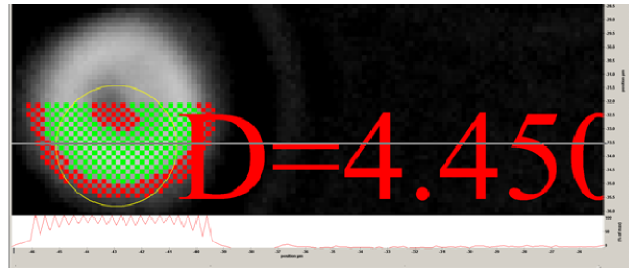

Figure 13. Particle segmentation image. AOI: 500%.

Further analysis with the same particle was done without the algorithm normalizing the images, which essentially provided lower global threshold values. At 80% AOI expansion, now the particle size is estimated as 6.72 µm in Figure 14.

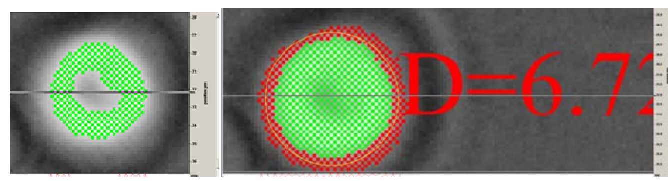

Figure 14. Global and particle segmentation, no normalization.

Note that the particle detection algorithm provides sizing with high-accuracy if appropriate parameters are used. However, it is impossible to process thousands of images with different parameters for different particles. A more universal detection and sizing algorithms are required to process shadowgraphy images.

Figure 15 demonstrates that if the particles are in the object plane, the current sizing algorithm can accurately predict the diameter of particles as small as 1 µm. Figure 15a shows the shadow of a particle 1 µm in diameter and Figure 15b is of a 2 µm diameter, both are in the object plane. The calculated diameters with the current algorithm are 1.798 µm and 2.66 µm, respectively. The software estimated diameter was consistently higher by an amount of about 0.7 µm. This offset was also observed for particles of diameters 3, 4, 5, 6, and 10 µm. The intensity profiles of the inverted shadow images are also shown in Figure 15 with the 0 to 100% normalized intensity scale shown on the right.

Axial and radial velocity profiles: The velocity measurements with micro-shadowgraphy in general provide high-accuracy. Possible errors however could result from the following sources: 1) a difference between the set and actual time delay between frames, 2) a difference between the calculated and actual particle centers in both frames, 3) incorrect camera field of view to pixel calibration, 4) small particle displacements between the frames, and 5) incorrect selection of pairs of particles between the frames. To verify the time delay, the laser pulse separation was measured with a fast photodiode and an oscilloscope. It was observed that the set delay time was always lower than the actual time between the pulses by 50 ns. For a total particle displacement of 50 µm, this introduced an increased velocity error of about 8%. The particle displacement between the frames was kept higher (~ 50 µm) using higher delay time settings to ensure negligible impact of incorrect particle center-detections. The calibration of the camera pixels using a length standard in the object plane was also verified before and after the experiments to ensure accuracy in the velocity calculations. Finally, to avoid incorrect particle pairing, a diameter restriction was applied between the particles in two frames.

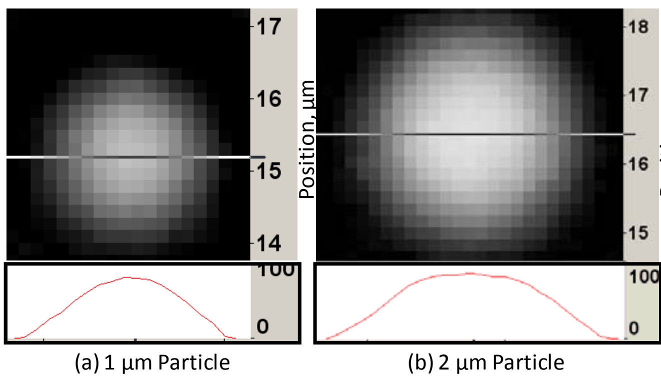

Figure 15. Inverted shadow images and centerline intensity profiles of particles in the object plane.

The axial velocity and the particle density graphs are shown in Figure 16. The plot shows the beam center is shifted towards the negative radial location between -10 µm and -5 µm. This shift was done intentionally to ensure that the fit line on the radial velocity plot goes through the origin. This indicates zero radial velocity at the center of the aerosol beam. Figure 17 shows the radial velocity distribution of all the particles.

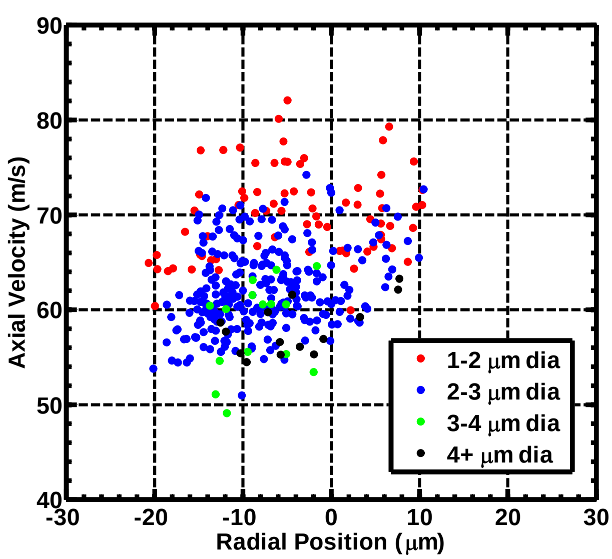

Figure 16. Axial velocity plot.

The magnitude of radial velocities increases with radial position. Figure 16 shows that the maximum radial velocity of 1.2 m/s corresponds to the farthest radial location at 20 µm. The linear trend is expected, although a large data-scatter can be seen. The data requires further verification with the corrected depth of field of the imaging system. As mentioned earlier, the radial velocities are only the projections of the actual velocities if the particles are located off of the object plane of the imaging system in the z-direction.

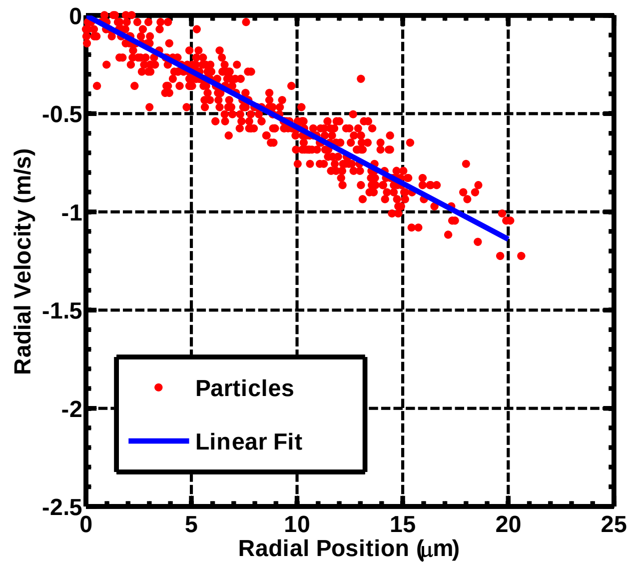

Figure 17. Radial velocity plot.

5. DEVELOPMENT OF THE PARTICLE SIZING ALGORITHM

Summarizing the discussion above, the current algorithm works well for particle velocity measurements; however the particle sizing algorithm needs to be revised to accurately size small particles (< 5 µm).

The sizing method is in question for the LaVision micro-shadowgraphy system, mainly due to the errors associated with diffraction around the particles. Figure 18 shows how the inverted particle image changes for the particle behind the object plane, in the object plane and in front of the object plane of the imaging system. The inverted shadow images show distinct features associated with whether the particle is located on the positive or the negative side of the object plane. The images with sharp disks are observed at distances away from the object plane and camera; however the images between the object plane and the camera have more blurred edges. The corresponding diffraction pattern and intensity-slopes for the first and second images are shown in Figure 19 and correspond to expected diffraction patterns produced around a circular obstacle and projected into the object plane.

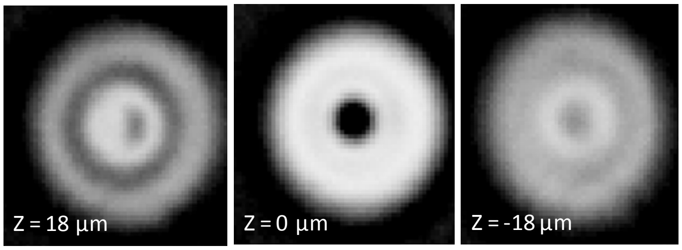

Figure 18. Shadow images at different depth of field.

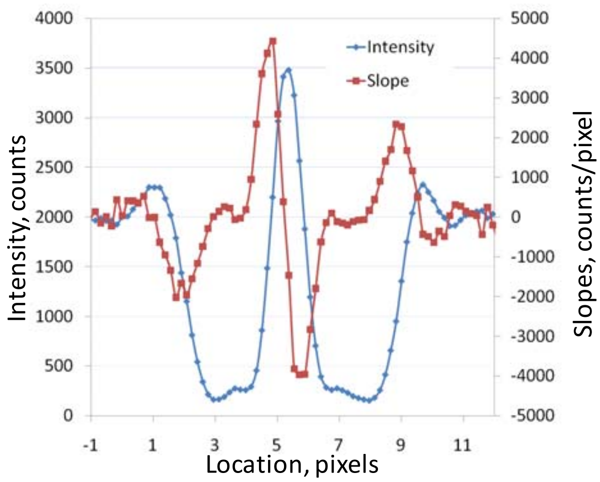

(a) Image at focal plane, z= 0

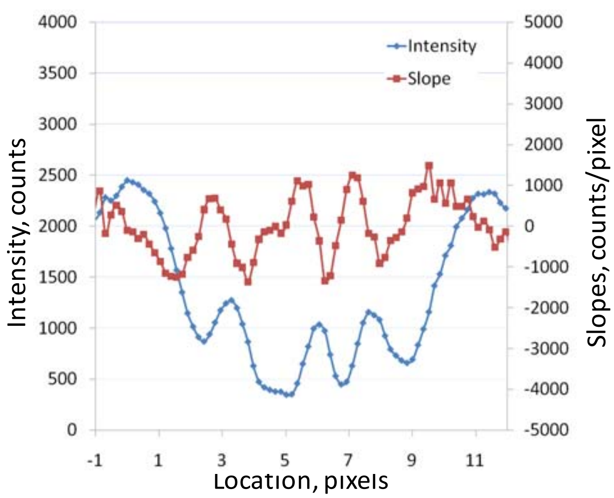

(b) Image at z = 18 µm

Figure 19. Intensity profiles of 6 µm particle at 0 and 18 µm from the object plane locations.

The figure shows the intensity profiles of the original shadow images as captured by the camera. The first profile near the object plane (*z*=0) shows sharp edges of the particle shadow, while the shadow image of the particle located at 18 µm beyond the object plane has edges slanted with a more disk like pattern as observed in Figure 18. The intensity-slopes of the diffraction pattern at the shadow edges become flatter as the particle distance increases in the *z*-direction. These average slopes can be calculated with the algorithm using the low-level and high-level diameters and the slope can then be used to predict the location of the particle in the *z*-axis.

The primary challenge with the existing algorithm was to capture the whole intensity profile at each particle location. A partial profile will end up with the smaller particle sizes as shown in figures 12 and 13. A two-step global threshold can be used to capture the complete particle profiles. The first global threshold will be applied to eliminate possible background noise, then the second threshold value (lower than the first) can be used to capture the central crests/dips of the shadows, Once these central crests are detected, a high Area of Interest (AOI) expansion (~ 200%) can be used to ensure that the complete particle shadows are detected.

The existing algorithm can be used to find the low and high-level areas of the detected particles to estimate the diameters. However, a detailed diffraction correction has to be applied to ensure accurate sizing of the particles irrespective of their apparent shadow size at different fields of view.

The present research investigated the particle profiles and apparent change in sizes with varying *z*-location for known particles of diameters 1, 2, 3, 5, 6 and 10 µm. The polystyrene particles of known sizes were put on a slide that was mounted on a precision translation (~1 µm resolution) stage. The slide was traversed at 1 µm steps from a location near the camera along the positive *z*-axis away from the camera until images could be detected. This ensured the complete range of the measurement volume was explored. For larger particles (6 and 10 µm), the step sizes used were 3 and 5 µm respectively. Depending on the actual particle diameters, the measurement range varies non-linearly. However a correlation can be made with the following data: 1) the actual particle size versus *z*-axis position calibration, 2) the detected particle diameter, 3) the intensity profiles, and 4) the intensity-slopes with the foot-prints of the particle-shadows indicating the image diameter as observed from the shadow images. This correlation can be applied to detect actual particle sizes smaller than 1 µm.

6. CONCLUSIONS

The experimental characterization of an aerosol flow through a micro-capillary of exit diameter 125 µm and length 1 cm, at high-speeds of ~70 m/s were conducted. A LaVision Inc. micro-shadowgraphy system was used to investigate the aerosol particle-size, velocity and number distributions. The state-of-the-art particle sizing techniques available today are still incapable of measuring smaller particles (~ 1 µm diameter) that flow at high-speed (greater than 50m/s). The existing algorithm for the velocity measurement works well and was able to provide an accurate velocity distribution of the aerosol flows, however the particle sizing based on the 2-D planar data obtained from a 3D measurement volume requires extensive modification of the existing algorithm. Sizing becomes difficult with smaller particles due to the complex diffraction pattern as imaged via the shadow images. The current algorithm with a highly restricted narrow depth of field can measure particle sizes with reasonable accuracy for particles of 5 µm or larger. The higher restriction on the detection algorithm is undesirable for the aerosol flow in the present study, because the particle density of the DW aerosol jet is low. Therefore, the present paper demonstrated the possible modification of the existing algorithm with less restriction on the detection parameters and more in-depth investigation of the depth of field correction for a wide range of particle sizes. The modified algorithm will use the predicted particle diameter, the intensity profiles, the intensity-slopes, and z-axis data to accurately size the particles. The new approach can be used to accurately size the particles of less than 1 µm in diameter.

ACKNOWLEDGEMENTS

This material is based on research sponsored by the Defense Microelectronics Activity under agreement number H94003-08-2-0801. The United States Government is authorized to reproduce and distribute reprints for government purposes, notwithstanding any copyright notation thereon.

REFERENCES

[1] J. P. Mitchel and M. W. Nagel, 2004, "Particle Size Analysis of Aerosols from Medicinal Inhalers", Powder and Particle (Number 22), KONA, "pp. 32-65"

[2] K. K. B. Hon, L. Li, I.M. Hutchings, 2008, "Direct Writing Technology- Advances and Developments", CIRP Annals - Manufacturing Technology. Volume 57 (Number 2), "pp 601-620"

[3] A. H. Lefebvre, 1989, *Atomization and Sprays*, Hemisphere Publishing Corporation, ISBN 0-89116-603-3, "pp. 367-405", "Chap. 9"

[4] J. T. Kashdan, J.S. Shrimpton, A. Whybrew, 2007, "A Digital Image Analysis Technique for Quantitative Characterization of High-speed Sprays", Optics and Lasers in Engineering, Volume 45, Issue 1, "pp. 106-115"

[5] I.S. Akhatov, J.M. Hoey, O.F. Swenson, and D.L. Schulz, Aerosol Focusing in Micro-capillaries: Theory and Experiment, Journal of Aerosol Science, Volume 39, "pp. 691-709", 2008.

[6] I.S. Akhatov, J.M. Hoey, D. Thompson, A. Lutfurakhmanov, Z. Mahmud, O.F. Swenson, and D.L. Schulz, 2009, "Aerosol Flow through a Micro-capillary", *Proceedings of ASME 2009 2nd Micro/Nanoscale Heat & Mass Transfer International Conference*, MNHMT2009, December 18-21, Shanghai, China.

[7] I.S. Akhatov, J.M. Hoey, O.F. Swenson, and D.L. Schulz, 2008, "Aerosol Flow through a Long Micro-capillary: Focused Collimated Aerosol Beam", Microfluidics and Nanofluidics, Volume 5, "pp. 215-224"

[8] C.D. Meinhart, S.T. Wereley, 2003, "The theory of diffraction–limited Resolution in Microparticle Image Velocimetry", Measurement Science and Technology, Volume 14, "pp. 1047 - 1053"

[9] K. Breuer, 2005, "*Microscale Diagnostics Techniques*", Springer-Verlag Berlin Heidelberg, ISBN 3-540-23099-8, "pp. 51-60"

[10] C.D. Meinhart, S.T. Wereley, M. H. B. Gray, 2000, "Volume Illumination for Two-dimensional Particle Image Velocimetry", Measurement Science and Technology, Volume 11, "pp. 809 - 814"

[11] S. Stone, C.D. Meinhart, D. C. Tretheway, S.T. Wereley, 2003, "Out of Plane Spatial Resolution of Volume Illumination PIV Using a Compound Lens System", Fifth International Symposium on Particle Image Velocimetry, Busan, Korea, September 22 – 24, 2003

[12] K. S. Kim, and S. S. Kim, 1994, "Drop Sizing and Depth of Field Correction in TV Imaging", Atomization and Sprays, Volume 4, "pp. 65 - 78"

